Fatigue criteria for short fiber-reinforced thermoplastic validated over various fiber orientations, load ratios and environmental conditions

Prashanth Santharam, Yann Marco, V. Le Saux, Matthieu Le Saux, Gilles Robert, Ida Raoult, Camille Guévenoux, Denis Taveau, Pierre Charrier

Fatigue criteria for short fiber-reinforced thermoplastic validated over various fiber orientations, load ratios and environmental conditions

P. Santharam[a,b], Y. Marco[a,*], V. Le Saux[a], M. Le Saux[a], G. Robert[c], I. Raoult[d], C. Guévenoux[d], D. Taveau[b], P. Charrier[b]

[a] *ENSTA Bretagne, UMR CNRS 6027, IRDL, F-29200, Brest, France*
[b] *Vibracoustic – CAE Durability Prediction Department, 44474, Carquefou, France*
[c] *Solvay Engineering Plastics, 69457 Lyon, France*
[d] *Groupe PSA – Direction Scientifique et des Technologies Futures, 78943 Vélizy–Villacoublay, France*

Abstract

Design of reinforced plastic parts against fatigue failure has become a serious issue these last few years for increasing engineering field applications. This is indeed a complex problem due to the strong anisotropy induced by the orientation of the fibers during the injection process and to the non-linear dissipative behavior of the matrix. This generates strong influences of numerous parameters (fiber orientation, environment, strain rate, load ratio, ...), which complicates both the description of the constitutive response and the definition of a robust and efficient fatigue criterion. This paper presents a very wide fatigue database (480 tension-compression tests) obtained on Polyamide 66 reinforced with 50% of glass fibers (PA66 GF50), for an extended range of load ratios (from -0.5 to 0.7), three orientations from the injection direction ($0°, 45°, 90°$) and two environmental conditions (50% humidity ratio and 80°C, 80% humidity ratio and 23°C). Beyond these experimental results, the goal of this paper is to compare the ability of numerous fatigue criteria to provide a robust description of the fatigue database, possibly with a unified set of parameters. Classical models as well as very recent ones are discussed and two variants of a new fatigue criterion are finally defined. This criterion is able to describe very accurately the full database with only four parameters. Finally, a focus is given to determine the minimal amount of experimental

*Corresponding author. E-mail address: yann.marco@ensta-bretagne.fr

data needed to obtain a reliable description of the fatigue results, on the full ranges of load ratios, orientations and environmental conditions.

Keywords: Creep-fatigue criterion, Short fiber-reinforced thermoplastic, Environment, Load ratio, Anisotropy

---

Nomenclature

$\bar{\sigma}_a$	Normalized nominal stress amplitude
$\bar{\sigma}_{max}$	Normalized nominal maximum stress
$\bar{E}_s$	Normalized secant modulus
$\dot{\varepsilon}_m$	Cyclic mean strain rate
$\dot{\varepsilon}^{\star}_m$	Cyclic mean strain rate at mid-life
σ	Nominal stress
σ_a	Stress amplitude
σ_m	Mean stress
σ_U	Ultimate tensile strength
Θ	Angle from the injection direction
ε	Nominal strain
ε_m	Cyclic (ratcheting) mean strain
N	Number of cycles
$N_{f,cal}$	Calculated number of cycles to failure
$N_{f,exp}$	Experimental number of cycles to failure
R_σ	Load ratio
T	Temperature
T_g	Glass transition temperature

W_{cr} Cyclic creep energy density per cycle

$W_{cr}^{\star}$ Cyclic creep energy density per cycle at mid-life

W_c Cyclic energy density per cycle

$W_c^{\star}$ Cyclic energy density per cycle at mid-life

W_e Elastic strain energy density per cycle

$W_e^{\star}$ Elastic strain energy density per cycle at mid-life

W_h Hysteresis energy density per cycle

$W_h^{\star}$ Hysteresis energy density per cycle at mid-life

1. Introduction

Short glass fiber-reinforced thermoplastics (SFRP) are widely used for structural automotive components such as chassis bushings or motor mounts, as they proved to be a cost-efficient solution combining sufficient stiffness for lower weight, to large freedom of shapes and high pace production thanks to the injection process. Cost and stiffness constraints usually lead to choosing polyamide matrices reinforced with glass fibers. Nevertheless, the efficient design of these parts against fatigue remains highly challenging mainly because of two points. The first one is the strong anisotropy induced by the orientation of the fibers during the injection process. As stiffeners and ribs are mandatory to improve the stiffness of these parts, complex microstructure and mechanical fields are superimposed, which leads to a difficult evaluation of local failure criteria [1–5]. The second difficulty comes from the non-linear dissipative behavior of the matrix, that is dependent on service conditions (humidity, temperature) and involves viscous features leading to hysteresis and cyclic ratcheting [6–9]. The combination of these two points generates strong influences of numerous parameters (fiber orientation [10, 11], environment [8, 12–14], strain rate [15, 16], load ratio [14, 17–19]) which complicates both the description of the constitutive response [20] and the definition of a robust and efficient fatigue criterion [21–23]. This paper is focused on the definition of the fatigue criterion but both aspects are clearly connected, as the fatigue indicators used in the model need to be described by the constitutive model.

A first range of fatigue criteria is based on stress components that are the usual inputs for samples as the tests are often force-driven for these stiff materials, or are obtained from structural computations possibly throughout simple constitutive models. These criteria often include stresses divided by the ultimate stress to failure under monotonic tensile stress, for the given tested condition (orientation, relative humidity, temperature, ...) [10, 11, 21]. These improved stress-based criteria seem to provide a reasonable agreement, and the advantage is that a quite simple constitutive model can be used to provide the input needed, as cyclic data are not required. Nevertheless, a single set of parameters cannot describe the influence of the load ratio and additional functions are needed to catch the effect of ratcheting, leading to cycle creep failure [18, 21, 24–26]. A second range of criteria relies on the assumption that the constitutive response during fatigue loading will reach a stationary state [27, 28]. In this state, the evolutions of the typical cyclic features (secant modulus, hysteresis, cyclic strain increment, cyclic energy density, dissipated energy density) are stabilized. Most of the fatigue criteria then base the analysis on one of these features: cyclic creep increment [29, 30], elastic strain energy-based [31, 32], dissipated energy [21, 33–35]. The results are indeed quite promising in most cases and a unification of the fatigue data for several orientations and environments is found, as well as for load ratios, usually over a limited range. The main weakness of these models is indeed their ability to describe accurately both negative load ratios and very positive ones. This is quite natural, as criteria based on the cyclic creep increment will not be able to describe negative load ratios (where almost no ratcheting occurs) while criteria based on the cyclic loop will fail to describe high positive load ratios, exhibiting a significant ratcheting and inducing an earlier failure. More recently, some criteria combining cyclic creep increment and cyclic energy density have been proposed [23, 36]. These studies provide a visible improvement to describe accurately, with a single set of parameters, the influences of orientation, load ratio and environment. Nevertheless, one should keep in mind that this approach requires a much finer description of the constitutive response and more complex models [20, 37–40] to be used in a design approach. It is therefore of primary importance to determine what are the optimal (*i.e.* minimum) cyclic features to be described accurately by constitutive models. A last range of fatigue criteria bases the analysis on the progressive increment of a damage variable [41–43]. These models are interesting as damage is obviously present in these materials, induced by their heterogeneous nature [29, 44, 45]. Nevertheless, two main drawbacks

are limiting their use. The first one is the need to identify clearly the damage contribution to the macroscopic response, which is not easy for these materials, as viscous effects also induce a drop of the secant modulus and because the damage is anisotropic [41]. The second point is the need to simulate the full fatigue lifetime, which is clearly difficult for industrial applications in the case of these highly non-linear materials.

This study follows three main objectives. The first one is to present the very wide experimental database on PA66 GF50 (polyamide 66 reinforced with 50% in mass of glass fibers). Over 480 fatigue tests have been performed on tensile specimens for an extended range of load ratios (from -0.5 to 0.7), three orientations $(0°, 45°, 90°)$ and two environmental conditions (relative humidity RH50% and temperature T80°C; relative humidity RH80% and temperature T23°C). The second objective is to compare the ability of numerous fatigue criteria to provide a robust description of the fatigue database, possibly with a unified set of parameters. Models based on stress components as well as typical cyclic features are considered. Furthermore, two original models, based on the combination of the creep energy density and of an evaluation of the cyclic (elastic or anelastic) energy are formulated and their performances are compared to other models. The goal is to determine which criteria can provide a unified set of parameters to describe the influences of orientation, environment and load ratios. If a unified set of parameters cannot be identified, the ranges of relevance for the criteria are discussed. One of the outcomes of this comparative study is also to determine what are the optimal cyclic features needed as a criterion input, that constitutive models should aim at. Finally, the original criterion combining creep energy density and cyclic energy density is selected, because with only 4 parameters, it unifies over 90% of the full experimental database within a scatter of factor 3. For this model, the last question investigated in this paper regards the downsizing of the database needed for the relevant identification of the criterion parameters. A last section therefore investigates the minimum experimental database (atmospheric conditions, load ratios and orientations) needed for the parameters identification, to describe accurately the full database.

The outline of the paper is as follows. Section 2 presents the material used, the experimental procedures and the experimental database. The typical cyclic mechanical features followed during the test are also introduced (secant modulus, hysteresis energy density, cyclic energy density, cyclic strain increment, creep energy density, elastic strain energy density). Section 3 presents

the evolutions of these parameters during the fatigue tests and sums up the fatigue lifetime obtained for the extended database. Section 4 presents various criteria from the literature and their ability to describe the full database, for both with or without a unified set of parameters. This section also defines and discusses two variants of an original fatigue criterion (called IDAFIP). In the final section 5, the criteria performances on several ranges of orientations, environments and load ratios are discussed. Furthermore, a discussion on the minimum database needed to identify the IDAFIP criterion parameters and still providing a good description of the full database is presented.

2. Material and experimental procedures

2.1. Material and samples

The material investigated is a PA66 GF50, produced by Solvay Engineering Plastics under the commercial name Technyl® A218V50. The cut was achieved for three different orientation angles, $\Theta = 0°$, $45°$ and $90°$, from the injection direction, as shown in Fig. 1. The gate used and the cutting area (far from both ends of the plate) insure that the orientation is homogeneous from one sample to another. The injection process induces a microstructure gradient along the thickness of the plate (skin/core effect), as illustrated from the profile of the a_{xx} component (along the injection direction x) of the second-order orientation tensor in the central section, also provided in Fig. 1.

2.2. Environmental conditions

The fatigue experimental database are generated for two atmospheric conditions, RH50% T80°C and RH80% T23°C, because they are representative of the conventional atmospheric conditions experienced by motor mounts and chassis mounts respectively. Fig. 2b compares the mechanical response obtained for these two conditions to standard conditions (RH50% T23°C). For the three considered orientation, the lower the distance to the glass transition, the stiffer the material response and the later the occurrence of the non-linear response. A convenient way to describe the influence of the thermo-hygrometric conditions on the mechanical properties, is to use the difference between the temperature of the test and the glass transition temperature T_g that depends on the water content and thus on the conditioning humidity ratio [6, 47]. Fig. 2a illustrates that the two conditions considered for the fatigue campaign are in the range of temperature $[T_g + 30°\text{C}; T_g + 45°\text{C}]$.

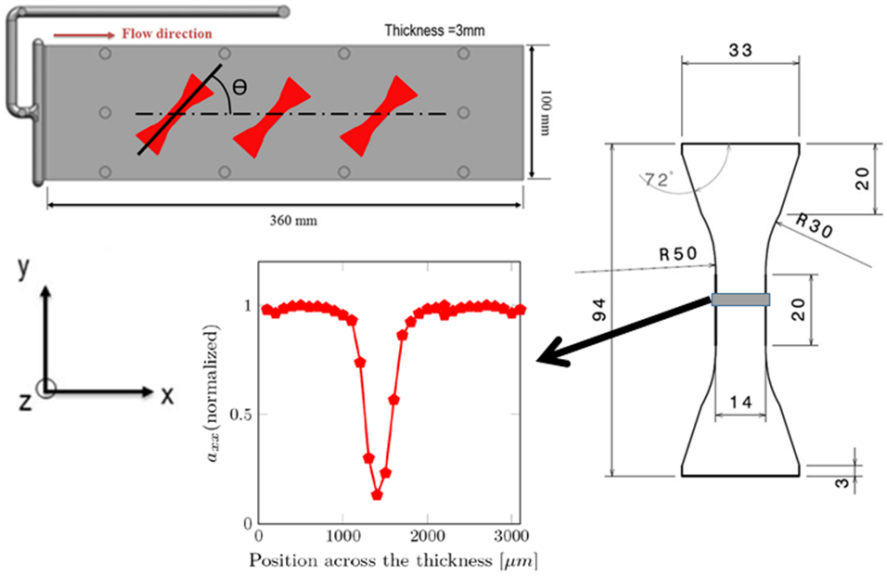

Figure 1: Dogbone specimens extracted from a PA66 GF50 injection-molded plate with their gauge length oriented at $\Theta = 0°$, $45°$ and $90°$ from the injection direction (dimensions in mm); through-thickness evolution of the a_{xx} component (along the injection direction x) of the second-order orientation tensor in the central section of the plate (data obtained from micro-tomography analysis [46]).

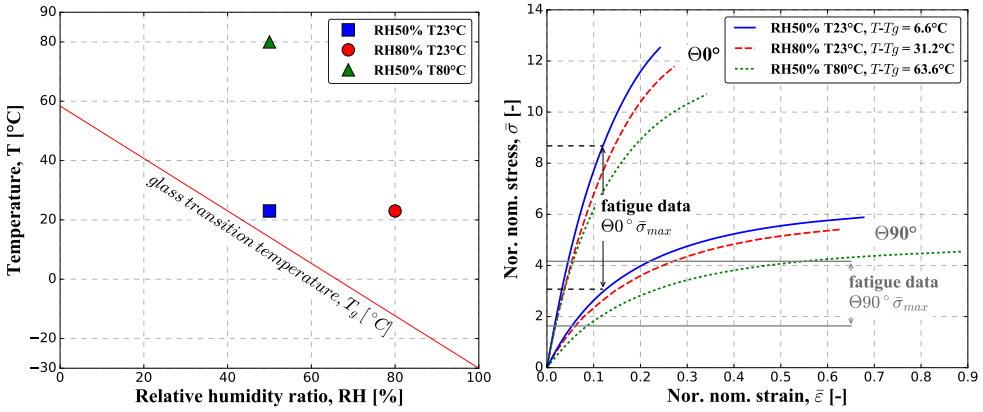

(a) (b)

Figure 2: (a) Evolution of the glass transition temperature of PA66 with atmospheric conditions. (b) Results of uniaxial tensile tests performed with similar stress rates for different atmospheric conditions.

Since PA66 GF50 is sensitive to atmospheric conditions, it is mandatory to regulate the atmospheric condition during the tests, which is ensured by the use of a Weiss climatic chamber. Moreover, the samples were conditioned as per the standards of Solvay Engineering and Plastics, to make sure that the samples are pre-conditioned to the required humidity concentration.

2.3. Test procedures

All the data presented in the article were obtained at Solvay Engineering Plastic, France. Two servo hydraulic machines (MTS 319.02 and MTS 370.10) were used to perform uniaxial sinusoidal load-controlled fatigue tests at 3 Hz frequency until failure. To check that the dissipation under cyclic loading did not induce overheating, the temperature fields at the surface of the specimen were recorded using a FLIR X6540SC infrared (IR) camera during the test, thanks to the IR transparent window of the climatic chamber. The rise of temperature was always lower than 10°C.

In addition, two optical cameras (VIC-3D system) estimate the strain on the surface of the samples using stereo digital image correlation (DIC) technique. To provide the contrast needed for performing DIC, a random speckle pattern was applied by black and white spray paints. The strain was evaluated as the average value over the full 20 mm-long gauge length. As an alternative to DIC, contact extensometer (MTS 634.33F-01) with a

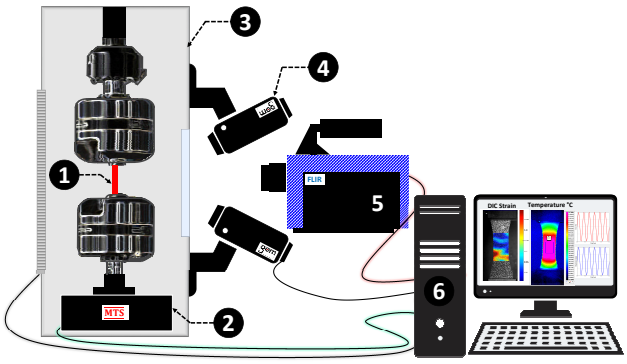

Figure 3: Experimental set-up: ① specimen, ② servo hydraulic machine, ③ climatic chamber, ④ optical cameras, ⑤ IR camera, ⑥ control and acquisition computer.

Env. conditions	Load ratio, R_σ					
	0.7	0.5	0.3	0.1	-0.2	-0.5
RH50% T80°C	0°, 45°, 90°	0°, 45°, 90°	0°, 45°, 90°	0°, 45°, 90°	0°, 45°, 90°	0°, 45°, 90°
RH80% T23°C	–	–	–	0°, 45°, 90°	0°, 45°, 90°	0°, 45°, 90°

Table 1: Conditions of the fatigue tests performed at 3 Hz frequency: environmental conditions, load ratios and angles between the loading direction and the injection direction.

12 mm-long gauge length was used for some of the experiments to determine the mean strain. An illustration of the experimental set-up is shown in Fig. 3.

2.3.1. Tests conditions

As mentioned earlier, the database was generated for three different orientations ($\Theta = 0°$, 45° and 90°) from the injection direction and for two environmental conditions (RH50% T80°C and RH80% T23°C). For the condition RH50% T80°C, the load ratios used are $R_\sigma = 0.7$, 0.5, 0.3, 0.1, -0.2, -0.5. In the case of condition RH80% T23°C, the database was generated for three load ratios: $R_\sigma = 0.1$, -0.2, -0.5. The summary of the tested conditions are given in Table 1. Approximately 20 tests with different stress amplitudes were performed for each configuration. In total, 480 tests have been achieved.

2.3.2. Thermomechanical quantities

Based on force and displacement measurements, the evolution of the mechanical response is analyzed along the fatigue tests (Fig. 4). Approximately

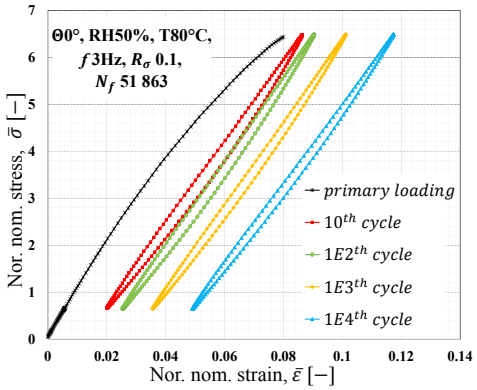

Figure 4: Example of stress-strain response obtained for several numbers of cycles during a cyclic test performed at 3 Hz, RH50% T23°C with a load ratio of 0.1 on a specimen oriented at $\Theta = 0°$ from the injection direction.

170 points were recorded per loop. The following mechanical quantities were calculated as illustrated in Fig. 5.

Secant modulus. The secant modulus E_s is determined from the slope of the cyclic response as illustrated in Fig. 5a and can be related to various phenomena (damage, viscoelasticity, viscoplasticity). For a given hysteresis loop at the N^{th} cycle, secant modulus can be estimated classically as follows:

$$E_s = \frac{\Delta\sigma}{\Delta\varepsilon} \tag{1}$$

where $\Delta\sigma$ and $\Delta\varepsilon$ are the amplitudes of the variations of nominal stress and strain over the cycle, respectively.

Cyclic mean strain rate. The local nominal strain in the gauge area is considered here, using DIC or contact extensometer. First, the minimum and maximum values for each cycle are calculated. The mean nominal strain ε_m is then determined (Fig. 5b). The evolution of this strain is, classically, nonlinear, and the slope, that defines the cyclic mean strain rate, is evolving along the fatigue cycle. In the following, the cyclic mean strain rate is evaluated as the slope of the mean strain at the N^{th} cycle:

$$\dot{\varepsilon}_m = \frac{d\varepsilon_m}{dN} \tag{2}$$

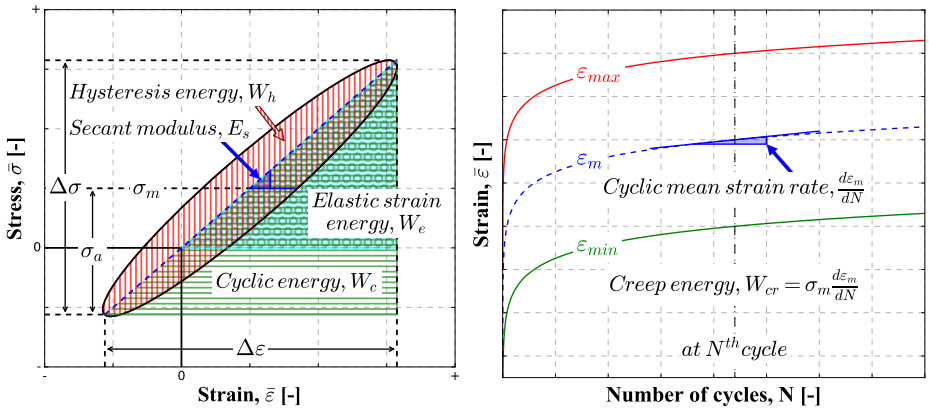

(a) (b)

Figure 5: Mechanical quantities determined from tests results: (a) secant modulus and cyclic, elastic strain and hysteresis energy densities; (b) cyclic mean strain rate and creep energy density.

Creep energy density. As evoked in the introduction, mean stress has a clear effect on the fatigue lifetime [14, 17–19], which is related to the plastic strain accumulation. In the following, criteria based on the combination of cyclic energy density to a parameter related to ratcheting will be suggested. In order to have similar kind of variables based on energy, it seemed therefore interesting to investigate an energy related to ratcheting. Several options exist in the literature dealing mostly with static creep [18, 21, 24–26]. In this study, the choice is made to formulate a creep energy density W_{cr} (more precisely cyclic creep or ratcheting energy) by multiplying the cyclic mean strain rate $\dot{\varepsilon}_m$ with mean stress σ_m:

$$W_{cr} = \sigma_m \dot{\varepsilon}_m \tag{3}$$

Hysteresis energy density. The hysteresis energy density is the anelastic energy density dissipated and/or stored by the material when subjected to cyclic deformation. For a given hysteresis loop at the N^{th} cycle, the hysteresis energy density can be calculated with Eq. 4. The hysteresis area was calculated using a trapeze method.

$$W_h = \int_{cycle} \sigma d\varepsilon \tag{4}$$

Cyclic energy density. For a given hysteresis loop at the N^{th} cycle, the cyclic energy density is related only to the cyclic amplitudes in strain ε and stress $\Delta\sigma$ [48]:

$$W_c = \frac{1}{2}\Delta\sigma\Delta\varepsilon \tag{5}$$

Elastic strain energy density. The elastic strain energy density per cycle W_e is defined as follows [31, 49]:

$$W_e = \left(\frac{1}{2}\Delta\sigma\Delta\varepsilon\right)^+ \tag{6}$$

The $^+$ exponent indicates that only the positive part of energy, associated with tensile stress, is considered, assuming that only this part is damaging. $W_e = W_c$ when $R_\sigma \geq 0$.

3. Experimental results

3.1. Evolution of mechanical quantities during fatigue cycles

The evolution during fatigue loading of the mechanical quantities defined in Section 2.3.2 is discussed hereinafter, for several load ratios R_σ, several normalized maximum stress levels $\bar{\sigma}_{max}$ and three sample orientations Θ from the injection direction. The values of stresses and secant moduli have been normalized by arbitrary values for confidentiality reasons. For each quantity, a single normalization factor is used throughout the whole paper. In the following, a bar is put on top of the symbol when the quantity is normalized. The strain fields were evaluated through the evolution of the profiles of strain occurrence over the gauge length. No localized effects have been highlighted, which support the average analysis achieved. The failure location occurs in the gauge length for most of the tests. Some failures occurred at the radius of the samples but it was decided to keep these data as they fall within the fatigue scatter.

The evolution of mechanical quantities are very similar for the two environmental conditions tested. For sake of clarity, the evolutions are shown only for the RH50% T80°C condition. As shown in Fig. 6, the normalized secant modulus $\bar{E}_s$ progressively decreases during cyclic loading, for all the load ratios and the orientations tested. This decrease in stiffness can have several physical origins (viscous and/or damage phenomena), *e.g.* evolution

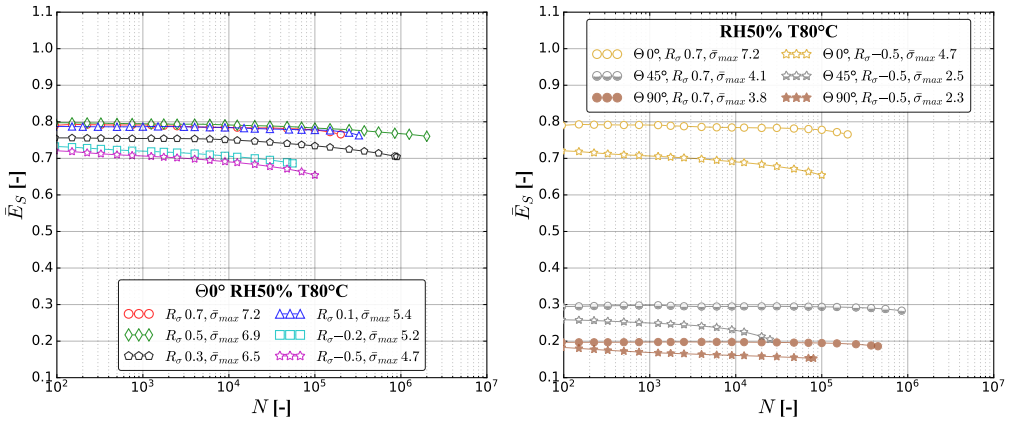

(a) (b)

Figure 6: Evolution of the normalized secant modulus as a function of the number of cycles until failure at RH50 T80°C: (a) several R_σ and $\bar{\sigma}_{max}$, for $\Theta = 0°$; (b) several Θ and $\bar{\sigma}_{max}$, for $R_\sigma = 0.7$ and -0.5.

of the structure of the semi-crystalline matrix, debonding between the matrix and the fibers or void nucleation at the fibers' ends. Nevertheless, in the absence of specific experimental observations, it is difficult to link this cyclic softening to a particular mechanism. The decrease in secant stiffness remains relatively small during most of the test, before failure initiation, indicating that potential damage remains confined and has little effect on the macroscopic response. As expected, the secant modulus tends to decrease when increasing the angle between the loading direction and the injection direction (Fig. 6b).

The cyclic mean strain (ratcheting strain) per cycle increases during cycling. As shown in Fig. 7, in accordance with the decrease of the cyclic mean strain rate $\dot{\varepsilon}_m = d\varepsilon_m/dN$, the cyclic creep energy density W_{cr} continuously decreases during cycling until failure, for all the conditions tested. The decreasing trend is the same for the three sample orientations tested (Fig. 7b). W_{cr} increases with increasing the load ratio for a given maximum stress level or with increasing the maximal stress level for a given load ratio, *i.e.* with increasing the mean stress level.

Fig. 8 shows examples of evolution of the hysteresis energy density per cycle W_h during fatigue tests. W_h decreases during the first cycles, then it tends to stabilize after a few cycles for the lowest load ratios tested to a few

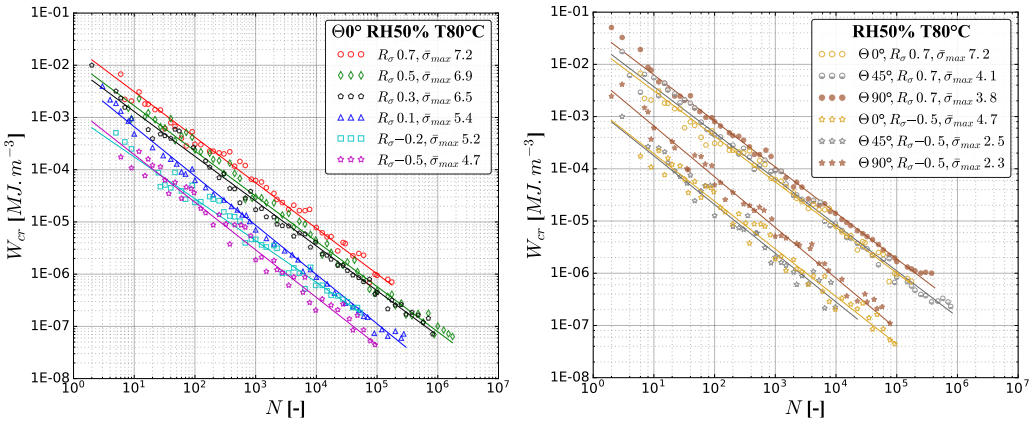

(a) (b)

Figure 7: Evolution of the creep energy density as a function of the number of cycles until failure at RH50 T80°C: (a) several R_σ and $\bar{\sigma}_{max}$, for $\Theta = 0°$; (b) several Θ and $\bar{\sigma}_{max}$, for $R_\sigma = 0.7$ and -0.5 (solid lines correspond to power-law fits).

hundreds of cycles for the highest load ratios, whatever the orientation of the sample from the injection direction. At equivalent lifespan, the higher the load ratio (and thus the lower the amplitude of the stress applied), the lower the hysteresis energy density (Fig. 8a). For given load ratio and lifetime, W_h does not significantly depend on sample orientation (Fig. 8b).

As shown in Fig. 9a, the cyclic energy density per cycle W_c first increases, before stabilizing after a few to a few hundreds of cycles. This tendency is consistent with the evolution of the secant modulus. Since the stress amplitude was maintained constant during the fatigue tests, the increase in W_c is due to an increase in strain amplitude during the cycles. This softening may be induced by an increase of the sample temperature and/or by a progressive damage. At equivalent fatigue lifetime, the lower the load ratio, the larger W_c, because the stress amplitude is higher. In Fig. 9b, the cyclic energy density once stabilized is nearly the same for 0°, 45° and 90° orientations, for one given load ratio, while the maximum stress level applied is not the same. This is due in particular to the difference in stiffness of the samples depending on the orientation from the injection direction.

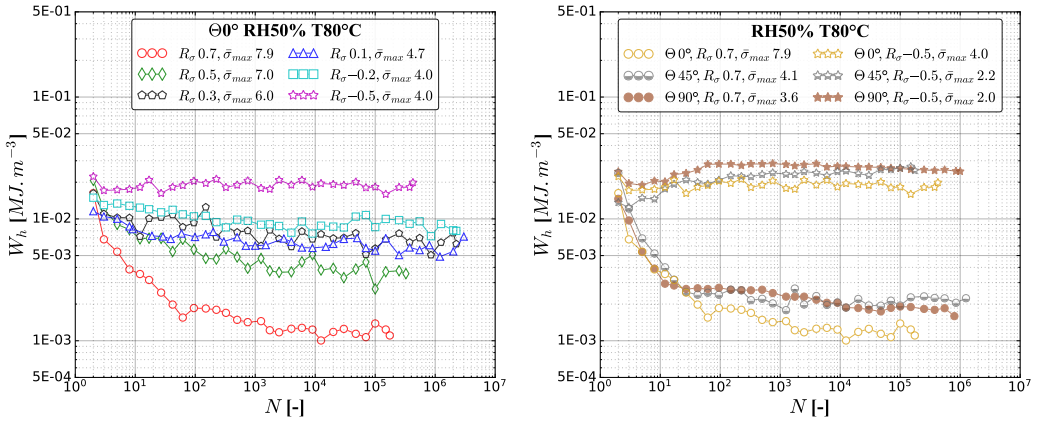

(a) (b)

Figure 8: Evolution of the hysteresis energy density as a function of the number of cycles until failure at RH50 T80°C: (a) several R_σ and $\bar{\sigma}_{max}$, for $\Theta = 0°$; (b) several Θ and $\bar{\sigma}_{max}$, for $R_\sigma = 0.7$ and -0.5.

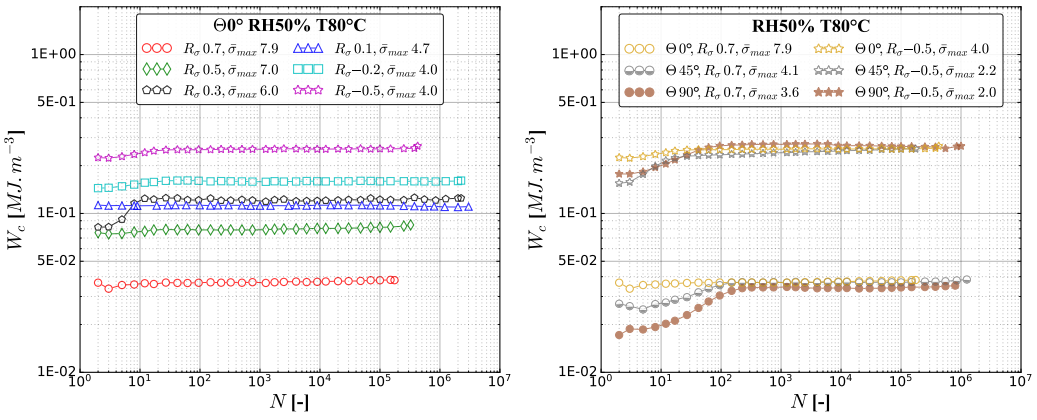

(a) (b)

Figure 9: Evolution of the cyclic energy density as a function of the number of cycles until failure at RH50 T80°C: (a) several R_σ and $\bar{\sigma}_{max}$, for $\Theta = 0°$; (b) several Θ and $\bar{\sigma}_{max}$, for $R_\sigma = 0.7$ and -0.5.

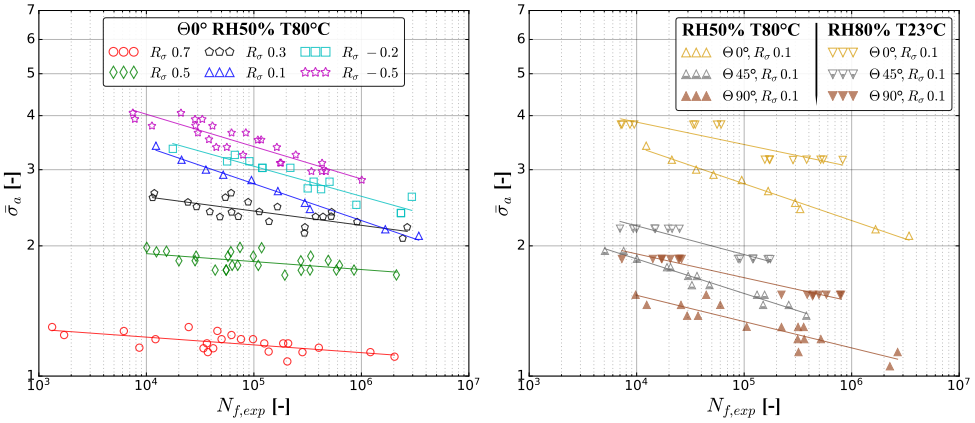

(a) (b)

Figure 10: Normalized nominal stress amplitude vs. number of cycles to failure: (a) several $\bar{\sigma}_a$, for $\Theta = 0°$ and RH50% T80°C; (b) several Θ and two atmospheric conditions, for $R_\sigma = 0.1$ (solid lines correspond to power-law fits, using one set of parameters for each condition).

3.2. Wöhler curves

Fig. 10 gives examples of normalized stress amplitude $\bar{\sigma}_a$ vs. experimental number of cycles to failure $N_{f,exp}$ curves (S-N or Wöhler curves) obtained for several load ratios, sample orientations and atmospheric conditions. Stress values have been normalized by one single arbitrary factor. For a given sample orientation, atmospheric condition and stress amplitude, the number of cycles to failure decreases with increasing the load ratio (Fig. 10a), *i.e.* the mean stress. All other parameters being equal, the fatigue strength (stress at which a given fatigue lifetime is obtained) is higher for the RH80% T23°C (*i.e.* $T - T_g = 30°C$) atmospheric condition than for the RH50% T80°C condition (*i.e.* $T - T_g = 45°C$), as illustrated for $R = 0.1$ in Fig. 10b. It is well-known that the fatigue strength of SFRP polyamides is sensitive to both temperature and relative humidity [11, 19, 26]. Dealing with the influence of orientation, the fatigue strength decreases when increasing the angle of loading from the injection direction, *i.e.* when decreasing the fraction of fibers aligned along the loading direction, as already observed in [10, 23] for example.

4. Fatigue criteria

The objective is to propose a fatigue criterion, with a limited number of parameters, able to unify the data that have just been presented, for all loading orientations with respect to the injection direction, load ratios and atmospheric conditions. Several fatigue criteria, existing in the literature or proposed in this paper, are examined in this section on the basis of the available database. Their ability to predict the fatigue lifetime is discussed. It is worth noting that the paper has not the vocation to compare the predictive capacities of the criteria, but rather challenge their ability to unify the full database.

4.1. Criteria based on one variable

4.1.1. Stress-based criterion

Power-law criterion. The evolution of the stress amplitude σ_a as a function of the number of cycles to failure can be described by a Basquin-type power-law relationship:

$$\sigma_a = aN_f^b \tag{7}$$

where a is the fatigue strength coefficient and b is the Basquin exponent. This criterion is obviously not able to unify the data for all the orientations, load ratios and atmospheric conditions. The fits obtained by using one set of parameters a and b for each condition are shown in Fig. 10.

Fig. 11 shows S-N curves where the stress level has been normalized with respect to the corresponding Ultimate Tensile Strength σ_U, obtained from monotonic uniaxial tensile tests conducted until failure for the same orientation and atmospheric condition), as proposed in [10, 11, 22]. It appears that it is possible by doing so to account for the effects of atmospheric conditions and sample orientations and to unify the data in a single master curve for each load ratio. By replacing σ_a by σ_a/σ_U in the power-law relationship with N_f, it can be envisioned to use one single set of strength coefficient and exponent for all orientations and atmospheric conditions:

$$\frac{\sigma_a}{\sigma_U} = a_\sigma N_f^{b_\sigma} \tag{8}$$

As a first approach, one single set of a_σ and b_σ parameters may be tuned independently of Θ, $T - T_g$ and R_σ. Table 2 gives the percentage of fatigue life data (among all the available data) predicted by this criterion (and the ones that are discussed hereinafter) within scatter bands of factors 2, 3 and 5.

In this Table, it is indicated whether the parameters of the criterion depends on Θ, R_σ or $T - T_g$, or not. As expected, the number of cycles to failure is very poorly predicted by the criterion described by Eq. 8 when one single set of parameters is used (only 13% of the data are within a scatter band of a factor 3), in particular because the data obtained for the various load ratios cannot be unified.

As a second approach, the a_σ and b_σ parameters can be adjusted for each R_σ. The corresponding fits are shown in Fig. 11a. Fig. 11b compares the number of cycles to failure calculated using this criterion, $N_{f,cal}$, to the number of cycles to failure obtained experimentally, $N_{f,exp}$. Two Tables are given at the bottom right in this figure, as well as in the following figures where the estimated and the experimental number of cycles to failure are compared. As done in Table 2, the table on the left indicates whether the parameters of the criterion used depends (Y stands for Yes) on Θ, R_σ or $T - T_g$, or not (N stands for No). For example, in Fig. 11b, the parameters do not depend on Θ and $T-T_g$ but depend on R_σ. The table on the right gives the percentage of data (among all the available data) within scatter bands of factors 2, 3 and 5, marked in dashed, dotted ans solid lines in the figure 11b, respectively. These percentages are also given in Table 2. Although it obviously shows better prediction capability than the version with only one single set of parameters, the power-law criterion based on σ_a/σ_U with one set of parameters for each load ratio (*i.e.* 12 parameters to be adjusted in total, as indicated in Table 2) is not very efficient (only 64% of the data are within the scatter band of factor 3).

Modified Gerber criterion. Mallick and Zhou [18] proposed to use the following stress-based modified Gerber equation to account for the effect of load ratio on fatigue life:

$$\frac{\sigma_a}{\alpha\sigma_U} + \left(\frac{\sigma_m}{\beta\sigma_U}\right)^2 = 1 \tag{9}$$

where σ_m is the mean stress and α and β are parameters to be adjusted. σ_a and σ_U still denote the stress amplitude and the ultimate tensile strength, respectively. The normalization by σ_U allows to unify the data with respect to sample orientation and atmospheric condition. Fig. 12a gives an example of Haigh-type diagram, showing the fatigue lifetime as a function of the normalized stress amplitude versus the normalized mean stress. The prediction of the modified Gerber equation once the α and β parameters have been adjusted, independently of the orientation and the atmospheric condition, is

Criterion	Eqs.	Dependency			n_p	% data $\left[\frac{1}{n}, n\right]$			Figs.
		Θ	R_σ	T-T_g		$n=2$	$n=3$	$n=5$	
Power-law σ_a/σ_U	8	N	N	N	2	9.8	13.1	18.7	–
		N	Y	N	12	42.2	63.5	85	11
Mod. Gerber	9	N	N	N	4	41.0	62.7	80.5	12
Mod. Tsai-Hill	10,11	N	N	N	4	9.8	18.7	27.7	–
		N	Y	Y	42	61.1	79.4	90.9	13
Cyclic strain rate	12	N	N	N	2	52.5	75.3	92.9	–
		N	Y	N	12	70.5	88.0	96.1	14
Creep energy	13	N	N	N	2	39.0	60.8	87.1	–
		N	Y	N	12	82.2	94.9	98.3	15
Hysteresis energy	14	N	N	N	2	12.2	17.2	23.9	–
		N	Y	N	12	35.1	51.7	70.5	16
Cyclic energy	15	N	N	N	2	11.4	15.8	23.7	–
		N	Y	N	12	47.3	66.2	83.6	17
Klimkeit *et al.*	16,17	N	N	N	2	17.3	30.6	45.0	–
		N	Y	N	12	34.8	54.0	71.9	18
Raphael *et al.* var. 1	18	N	N	N	4	60.8	83.5	95.2	19
Raphael *et al.* var. 2	19,20	N	N	N	5	72.5	92.3	98.3	20
IDAFIP var. 1	21	N	N	N	4	75.2	91.9	98.8	21
IDAFIP var. 2	22	N	N	N	4	78.3	96.5	99.8	22

Table 2: Comparison of several fatigue criteria: dependency of the parameters to Θ, R_σ and $T - T_g$ (Y: Yes; N: No), total number of adjusted parameters n_p, percentage of data within scatter bands of factors 2, 3 and 5.

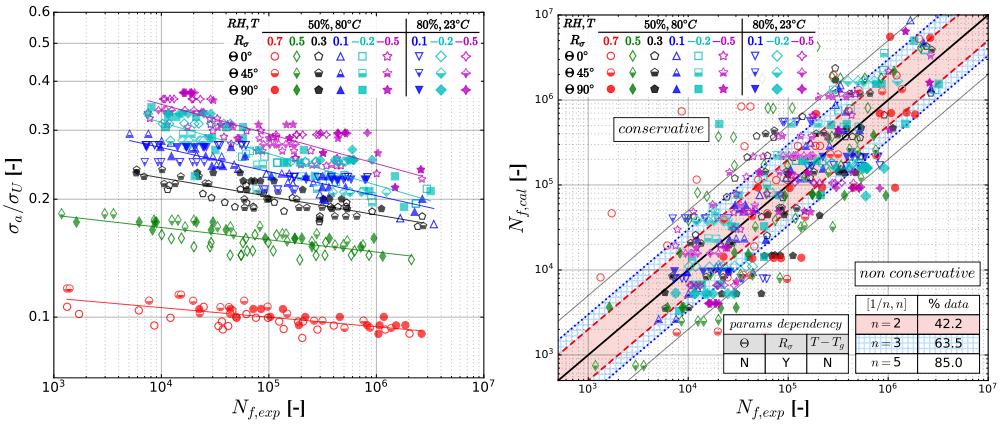

(a) (b)

Figure 11: (a) Nominal stress amplitude normalized by the corresponding σ_U vs. number of cycles to failure for several load ratios, two atmospheric conditions and three orientations (solid lines correspond to power-law fits, using one set of parameters for each R_σ). (b) Number of cycles to failure estimated using a power-law equation applied to σ_a/σ_U (one set of parameters for each R_σ) vs. experimental number of cycles to failure.

shown for several number of cycles to failure. The evolution of α and β as a function of the number of cycles to failure is shown in top right of Fig. 12a. α significantly decreases with increasing the number of cycles while β does not evolve much. In practice, the values of α and β can be determined for the desired lifetime and σ_a and σ_m can then be estimated from the modified Gerber criterion.

Fig. 12b compares the number of cycles to failure calculated using the modified Gerber equation to the experimental number of cycles. Again, the Tables at the bottom in the figure indicates the dependency of the parameters of the model to Θ, R_σ and $T - T_g$ and gives the percentage of data within scatter bands of factors 2, 3 and 5. These information are also given in Table 2. The modified Gerber equation appears to be able to represent the load ratio (*i.e.* mean stress) effect, in addition to the effects of sample orientation and atmospheric condition taken into account by normalizing σ_a and σ_m by σ_U. Nevertheless, the overall difference between $N_{f,cal}$ and $N_{f,exp}$ is quite large (only 63% are within the scatter band of a factor 3).

Modified Tsai-Hill criterion. Bernasconi *et al.* [10] and De Monte *et al.* [11] proposed to use the Tsai-Hill criterion adapted to cycling loading to predict

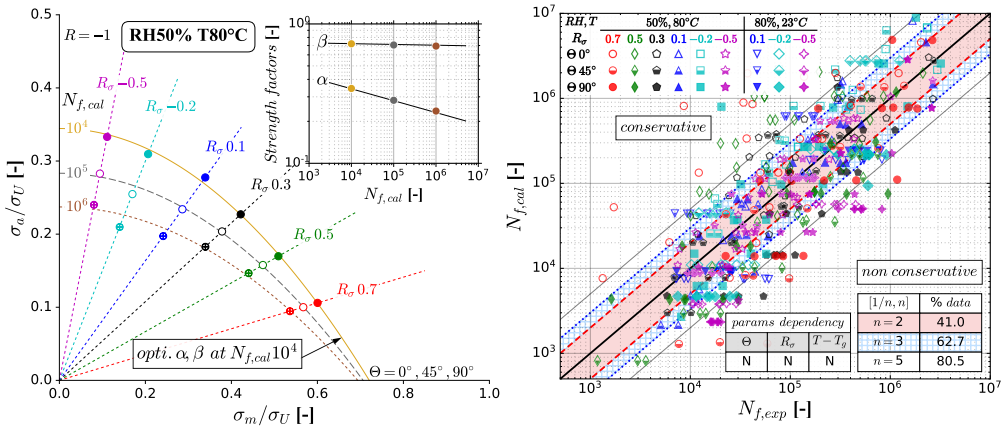

(a) (b)

Figure 12: (a) Haigh-type diagram for RH50% T80°C; prediction of the modified Gerber equation; evolution of the parameters of the modified Gerber equation with cycle number. (b) Number of cycles to failure estimated using the modified Gerber criterion vs. experimental number of cycles to failure.

fatigue failure and take into account the effect of fiber orientation with respect to the loading direction. This model can here be written as follows:

$$\left(\frac{\sigma_{0max}}{\sigma_{0u}}\right)^2 - \frac{\sigma_{0max}\sigma_{90max}}{\sigma_{0u}^2} + \left(\frac{\sigma_{90max}}{\sigma_{90u}}\right)^2 + \left(\frac{\sigma_{45max}}{\sigma_{12u}}\right)^2 = 1 \qquad (10)$$

with

$$\sigma_{iu}\left(N_f\right) = \sigma_{iu}\left(10^6\right)\left(\frac{10^6}{N_f}\right)^{\frac{1}{k}},\ i = \{0, 90, 12\} \qquad (11)$$

σ_{0max}, σ_{90max} and σ_{45max} are the maximum stresses applied during cyclic loading along the 0°, 45° and 90° orientations, respectively. $\sigma_{0u}\left(10^6\right)$, $\sigma_{90u}\left(10^6\right)$ and $\sigma_{12u}\left(10^6\right)$ correspond to the maximum stresses at $N_f = 10^6$ associated with σ_{0max}, σ_{90max} and σ_{45max}, respectively. $\sigma_{0u}\left(10^6\right)$ and $\sigma_{90u}\left(10^6\right)$ have been determined from S-N curves obtained for 0° and 90° orientations (Fig. 10). $\sigma_{12u}\left(10^6\right)$ has been optimized to fulfill equality in Eq. 10. The material parameter k corresponds to the inverse of the slope of the S-N curves.

As shown in Table 2, when using only one set of parameters $\sigma_{\Theta u}$ and k for all conditions, the modified Tsai-Hill criterion is not able to accurately predict the fatigue life of the material (only 19% of the data points are within a scatter band of a factor 3). To improve the estimations, the parameters

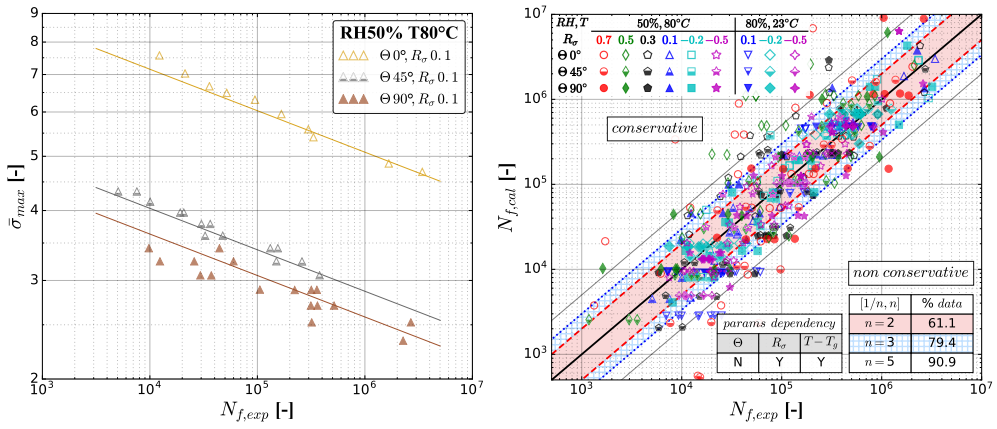

(a) (b)

Figure 13: (a) Normalized nominal maximal stress vs. number of cycles to failure, for $R_\sigma = 0.1$ and RH50% T80°C, for several Θ (solid lines correspond to power-law fits); (b) Number of cycles to failure estimated using the modified Tsai-Hill criterion (one set of parameters for each R_σ and $T - T_g$) vs. experimental number of cycles to failure.

can be tuned for each R_σ and $T - T_g$ (atmospheric condition). k does not significantly depend on Θ and $T - T_g$ (Figs. 10 and 13a) so that only the dependency on R_σ is to be taken into account. As shown in Fig. 13b, in this case, the modified Tsai-Hill model is able to describe the influence of orientation on fatigue life, for given load ratios and atmospheric conditions. This model leads to a better overall estimation of fatigue life (79% of the predicted fatigue lifetimes are within a scatter band of a factor 3) than the power-law criterion based on stress normalized by ultimate stress (64% the data within a scatter band of a factor 3, when one set of parameters is determined for each load ratio) or the modified Gerber model (63% within a scatter band of a factor 3). However, the parameters of the Tsai-Hill model have to be tuned for each atmospheric condition contrary to the model based on σ_a/σ_U and for each R_σ contrary to the modified Gerber criterion, so that 42 parameters have to be tuned in total, which is also not very convenient for application to industrial structures.

4.1.2. Cyclic strain rate and energy-based criteria

Cyclic mean strain rate. Fig. 14 shows the cyclic mean strain rate determined at mid-life, $\dot{\varepsilon}^\star_m = \dot{\varepsilon}_m\,(N_f/2)$, as a function of the experimental number of fatigue to failure, for the various conditions tested. The data are almost

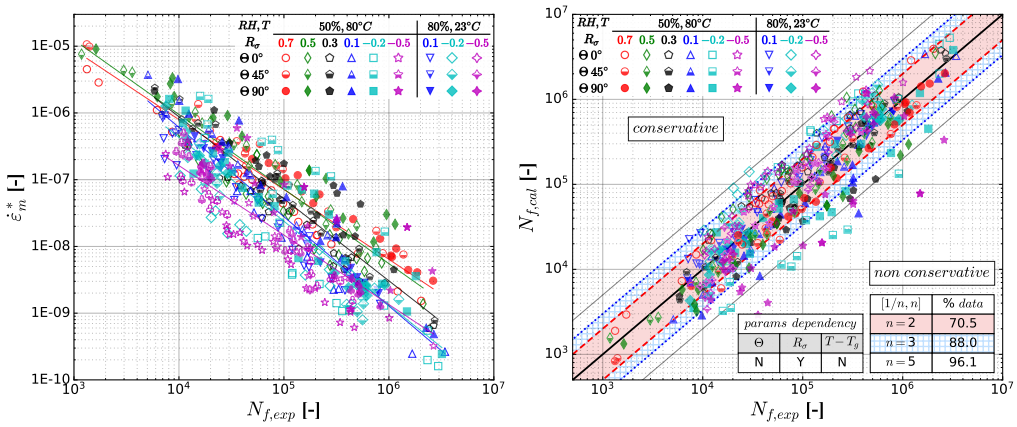

(a) (b)

Figure 14: (a) Cyclic mean strain rate at mid-life vs. number of cycles to failure for several load ratios, two atmospheric conditions and three orientations (solid lines correspond to power-law fits, using one set of parameters for each R_σ). (b) Number of cycles to failure estimated using a power-law equation applied to $\dot{\varepsilon}_m^\star$ (one set of parameters for each R_σ) vs. experimental number of cycles to failure.

grouped together regardless of the orientations and the atmospheric conditions. $\dot{\varepsilon}_m^\star$ does not manage to group the curves for different load ratios. It can be noticed that negative load ratios are set apart. The following power-law criterion based on $\dot{\varepsilon}_m^\star$ has been identified:

$$\dot{\varepsilon}_m^\star = a_{\dot{\varepsilon}} N_f^{b_{\dot{\varepsilon}}} \tag{12}$$

where $a_{\dot{\varepsilon}}$ and $b_{\dot{\varepsilon}}$ are material parameters. When one single set of parameters is used for all conditions, 75% of the fatigue lifetime data are predicted by the criterion within a scatter band of a factor 3 (Table 2).

When the parameters are adjusted for each load ratio, the estimation can be improved. The corresponding power-law fits are represented in Fig. 14a. Fig. 14b shows the lifetime estimated by applying the criterion with a set of parameters for each load ratio, independently of Θ and $T - T_g$. 88% of the predicted fatigue lifetimes are within a scatter band of a factor 3. As expected and evoked in the Introduction, the predictions are therefore pretty good for load ratios higher than 0.1 but poor for negative load ratios.

Creep energy density. Fig. 15 shows the cyclic creep energy density per cycle determined at mid-life $W_{cr}^\star = W_{cr}\,(N_f/2)$, as a function of the experimental

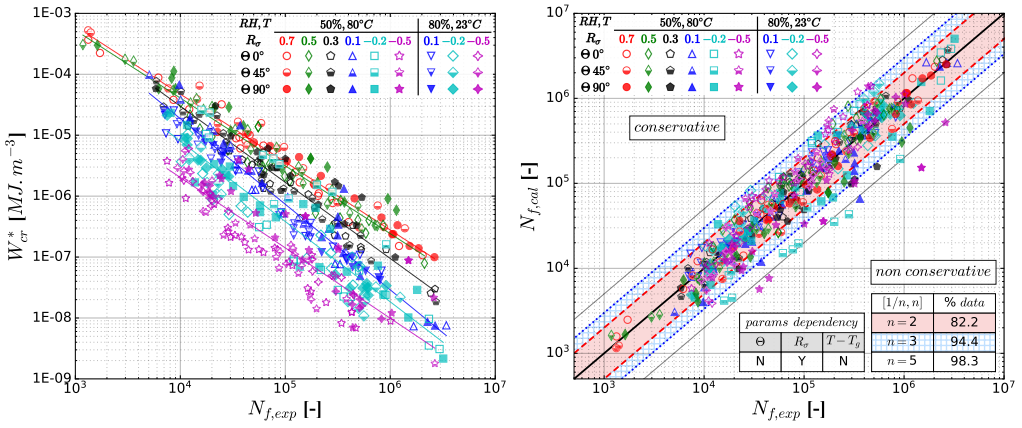

(a) (b)

Figure 15: (a) Cyclic creep energy density at mid-life vs. number of cycles to failure for several load ratios, two atmospheric conditions and three orientations (solid lines correspond to power-law fits, using one set of parameters for each R_σ). (b) Number of cycles to failure estimated using a power-law equation applied to $W_{cr}^{\star}$ (one set of parameters for each R_σ) vs. experimental number of cycles to failure.

number of fatigue to failure. The conclusions are very similar to that of $\dot{\varepsilon}_m^{\star}$. The creep energy density manages to group almost all data regardless of the orientations and the atmospheric conditions but fails to unify the tendencies for negative load ratios. The following power-law criterion based on $W_{cr}^{\star}$ can be identified:

$$W_{cr}^{\star} = a_{W_{cr}} N_f^{b_{Wcr}} \tag{13}$$

When a single set of parameters is identified, 61% of the database can be grouped within a scatter band of factor 3 (Table 2). This rather low percentage is related to the negative load ratios mostly. Conversely, when the parameters are dependent on the load ratio, 94% of the predicted fatigue lifetimes are within a scatter band of a factor 3.

Hysteresis energy density. Fig. 16 shows the evolution of the hysteresis energy density per cycle determined at mid-life $W_h^{\star} = W_h\,(N_f/2)$ as a function of N_f. It is worth noting that W_h stabilizes after a few hundred of cycles at most (Fig. 8), so that equivalent results (with different parameters) are obtained with a mean value of W_h evaluated for a reduced number of cycles. Several number of cycles have been investigated, ranging from $N_f/50$

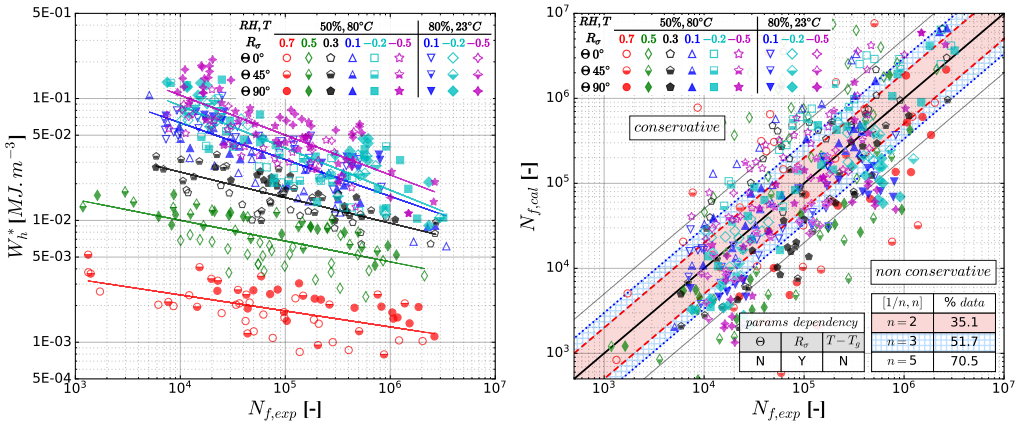

(a) (b)

Figure 16: (a) Hysteresis energy density at mid-life vs. number of cycles to failure for several load ratios, two atmospheric conditions and three orientations (solid lines correspond to power-law fits, using one set of parameters for each R_σ). (b) Number of cycles to failure estimated using a power-law equation applied to $W_h^\star$ (one set of parameters for each R_σ) vs. experimental number of cycles to failure.

to $N_f/2$. The parameters identified for the criteria are evolving but without changing the performance.

The data are almost grouped together for different sample orientations or atmospheric conditions but load ratios over 0.1 are clearly set apart. This confirms that fatigue criteria based on hysteresis energy density can be mostly efficient for zero and negative load ratios, as observed by Launay *et al.* [21] for $R_\sigma = -1$ and 0.

Power-law fits can be suggested as follows:

$$W_h^\star = a_{W_h} N_f^{b_{W_h}} \tag{14}$$

For a unified set of parameters, the criterion is not able to describe the full database as only 17% of the data points are within a scatter band of a factor 3 (Table 2). When using a different set of parameters for each R_σ, the prediction of fatigue life remains poor (only 52% of the data points are within a scatter band of a factor 3), which is mostly due to positive load ratios.

Cyclic energy density. Here, the cyclic energy density per cycle at mid-life $W_c^\star = W_c\,(N_f/2)$ is considered. W_c is stabilized after a few hundred cycles

at most (Fig. 9). As a consequence, values of W_c could have been considered for a smaller number of cycles. The observations made for $W_h^\star$ are almost the same for $W_c^\star$: the value of $W_c^\star$ at a given fatigue life does not significantly depend on either orientation or atmospheric condition; it depends on the load ratio, significantly when the load ratio is higher than 0.1, only slightly for lower load ratios (Fig. 17).

A power-law can be identified:

$$W_c^\star = a_{W_c} N_f^{b_{W_c}} \tag{15}$$

Very poor estimation is obtained by using one set of parameters for all conditions (16% of the data within a scatter band of a factor 3; see Table 2). The parameters a_{W_c} and b_{W_c} have then been adjusted for each load ratio, independently of Θ and $T - T_g$. The fatigue life predicted using this criterion is compared to the experimental data in Fig. 17b. Approximately 66% of the data are predicted within a scatter band of a factor 3, which is even slightly better than the estimation made with a power-law criterion based on $W_h^\star$. Furthermore, cyclic energy density has the advantage to be easier to calculate within a design loop since only the amplitudes of stress and strain are required, while an accurate evolution of stress as a function of strain curve over the full cycle is needed to calculate the hysteresis energy density.

Elastic strain energy density. On the basis of Kujawski and Ellyin' work [31], Klimkeit *et al.* [32] proposed a criterion based on elastic strain energy density per cycle W_e to estimate the fatigue life of SFRP thermoplastics subjected to multiaxial loading. The value of W_e is here taken at mid-life: $W_e^\star = W_e\,(N_f/2)$. As shown in Fig. 18a, $W_e^\star$ does not depend much on Θ and $T - T_g$ but strongly depends on R_σ, in particular for positive load ratios, in the same way as $W_c^\star$. The criterion proposed by Klimkeit *et al.* [32] can then be expressed as follows:

$$f_{W_e} W_e^\star = a_{W_e} N_f^{b_{W_e}} \tag{16}$$

where a_{W_e} and b_{W_e} are material parameters and f_{W_e} is a function of R_σ defined as follows to account for the effect of mean stress (*i.e.* load ratio).

$$f_{W_e}^2 - \frac{\sigma_m}{\sigma_a} f_{W_e} = 1 \tag{17}$$

As shown in Fig. 18b, the model leads to poor estimation of fatigue life (31% of the data within a scatter band of a factor 3; see Table 2). In particular,

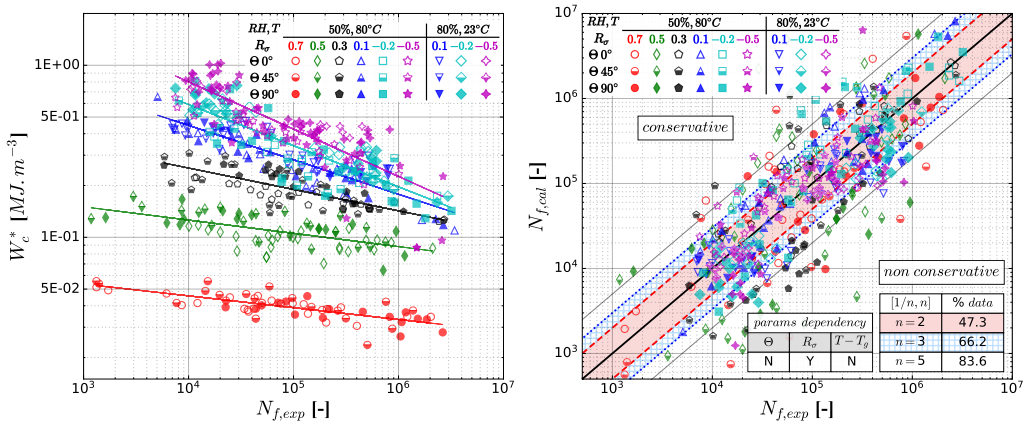

Figure 17: (a) Cyclic energy density at mid-life vs. number of cycles to failure for several load ratios, two atmospheric conditions and three orientations (solid lines correspond to power-law fits, using one set of parameters for each R_σ). (b) Number of cycles to failure estimated using a power-law equation applied to $W_c^\star$ (one set of parameters for each R_σ) vs. experimental number of cycles to failure.

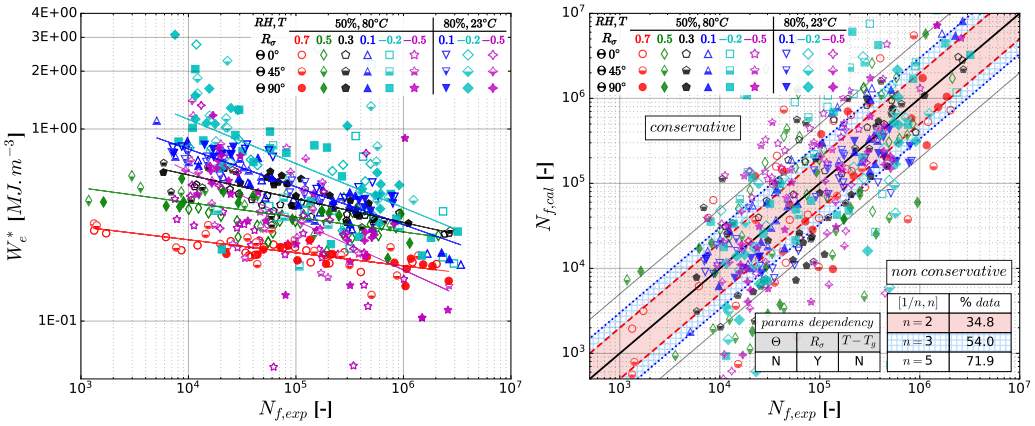

Figure 18: (a) Elastic strain energy density at mid-life vs. number of cycles to failure for several load ratios, two atmospheric conditions and three orientations (solid lines correspond to power-law fits, using one set of parameters for each R_σ). (b) Number of cycles to failure estimated using the Klimkeit's criterion [32] based on $W_e^\star$ and supposed to take into account the load ratio effect.

the effect of load ratio is badly reproduced. The estimation is improved if a_{W_e} and b_{W_e} are adjusted for each load ratio (54% of the data within a scatter band of a factor 3; see Table 2).

4.2. Criteria based on two variables

Two main conclusions can be drawn from the previous section. The first one is the inability of all the criteria based on a single variable to unify, with a single set of parameters, influences of load ratio, orientation and environmental condition. The second one is that a quantity based on the cyclic mean strain is able to capture the effects of these three parameters for positive load ratios, whereas a quantity based on cyclic energies either elastic or anelastic is able to capture the effects of these three parameters for negative load ratios. The objectives of the section is to consider criteria using both features. First, recent models from the literature [23] are considered. Then, two variants of a new model called IDAFIP are presented and evaluated.

It is worth introducing here that the way to present the results in the following is changed to better highlight the differences between the criteria. Two subplots per criterion are presented: on the left, the classic graphical representation with the predicted number of cycles to failure as a function of the experimental number of cycles to failure; on the right, the fatigue lifetime isolines in the plane of the mixed chosen variables.

4.2.1. Raphael's mixed criterion

Variant 1. Raphael *et al.* [23] recently proposed a simple criterion that combines the hysteresis energy density and the cyclic mean strain rate according to:

$$N_f = \min\left[A\left(\frac{\dot{\varepsilon}_m^\star}{\dot{\varepsilon}_0}\right)^n ; B\left(\frac{W_h^\star}{W_0}\right)^m\right] \tag{18}$$

where A, n, B, m are parameters, $\dot{\varepsilon}_0$ and W_0 are normalizing values and $\dot{\varepsilon}_m^\star = \dot{\varepsilon}_m(N_f/2)$ and $W_h^\star = W_h(N_f/2)$ are respectively the cyclic mean strain rate and hysteresis energy density at mid-life. Fig. 19a shows the prediction of this criterion that is good for all the testing conditions, with 84% of the data within the scatter bands of factor 3. However, the fatigue lifetime isolines, plotted in Fig. 19b, show that the transition between the domain governed by the cyclic strain rate and the one governed by the hysteresis energy density is too sharp.

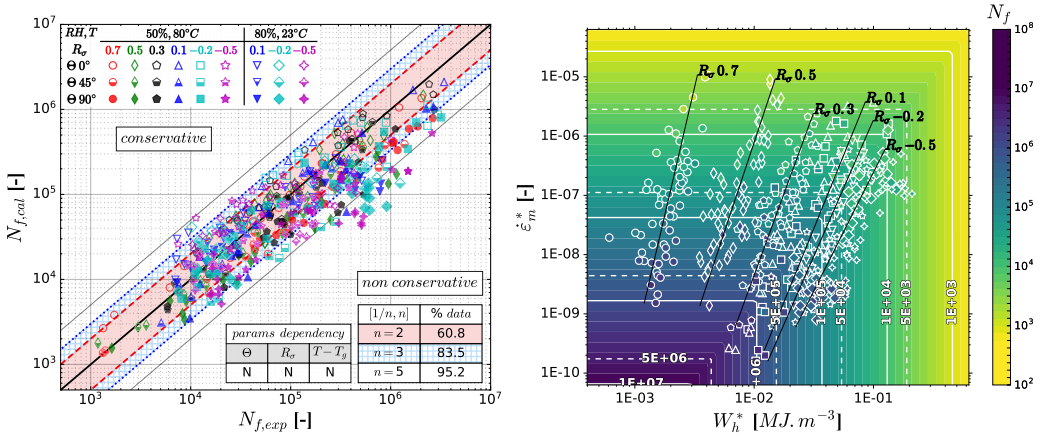

(a) (b)

Figure 19: Performance of the first variant (based on the minimum) of the mixed criterion proposed by Raphael *et al.* [23]: (a) comparison between the predicted fatigue life and the experimental one, (b) shape of the fatigue lifetime isolines.

Variant 2. Raphael *et al.* [23] proposed another version of the previous criterion by introducing a weight function, meant to smooth the transition between the areas respectively governed by cyclic strain rate and hysteresis energy density:

$$w = \frac{1}{2}\left(1 + \tanh\left[\gamma\left(\left[\frac{B}{A}\right]^{\frac{1}{n}} - \frac{\dot{\varepsilon}^\star_m}{\dot{\varepsilon}_0}\left[\frac{W^\star_h}{W_0}\right]^{-\frac{m}{n}}\right)\right]\right) \tag{19}$$

The criterion therefore writes:

$$N_f = (1-w)A\left(\frac{\dot{\varepsilon}^\star_m}{\dot{\varepsilon}_0}\right)^n + wB\left(\frac{W^\star_h}{W_0}\right)^m \tag{20}$$

For this variant, it has been chosen to follow the recommendations of the authors to set the initial values. The adjusted parameters values of the first criterion variant (Eq. 19) were used as initial values for the identification of the variant 2. The identification was then performed over the set of parameters without any sequenced analysis or weight functions, in a similar manner to other mixed criteria. Fig. 20a shows the prediction of this criterion. A significant improvement over the first variant is noticed, with 92% of the data within a scatter band of factor 3. Nevertheless, the weight function also

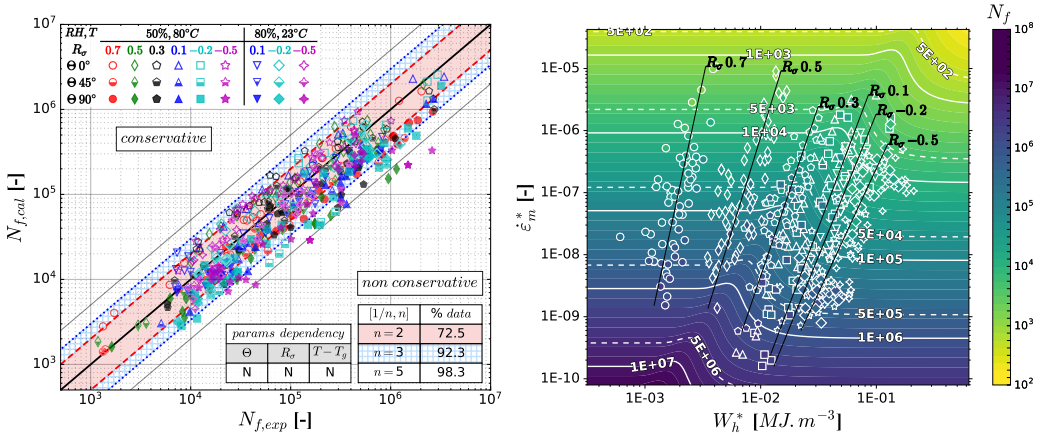

Figure 20: Performance of the second variant (based on the continuous criterion) of the mixed criterion proposed by Raphael *et al.* [23]: (a) comparison between the predicted fatigue life and the experimental one, (b) shape of the fatigue lifetime isolines.

induces non-physical evolutions for high hysteresis energy density values (see Fig. 20b).

4.2.2. New proposals of mixed formulations: IDAFIP criteria

In this section, two variants of an original energy-based mixed criterion called IDAFIP are proposed and confronted to the extensive experimental database available.

Variant 1. The first variant of the criterion is based on the creep energy density and on the hysteresis energy density according to

$$\frac{1}{N_f} = \left(\frac{W_{cr}^\star}{A_1}\right)^{b_1} + \left(\frac{W_h^\star}{C_1}\right)^{d_1} \tag{21}$$

The energetic quantities $W_{cr}^\star$ and $W_h^\star$ are evaluated at mid-life. A_1 and C_1 are normalizing parameters and b_1 and c_1 are dimensionless parameters. These four parameters are identified based on the entire experimental database and the results are presented in Fig. 21. More specifically, Fig. 21a shows the comparison between the computed fatigue lives and the experimental ones. The predictions are very good, with 92% of the data within a scatter band of factor 3. Moreover, the fatigue life isolines presented in Fig. 21b exhibit smooth and consistent evolutions.

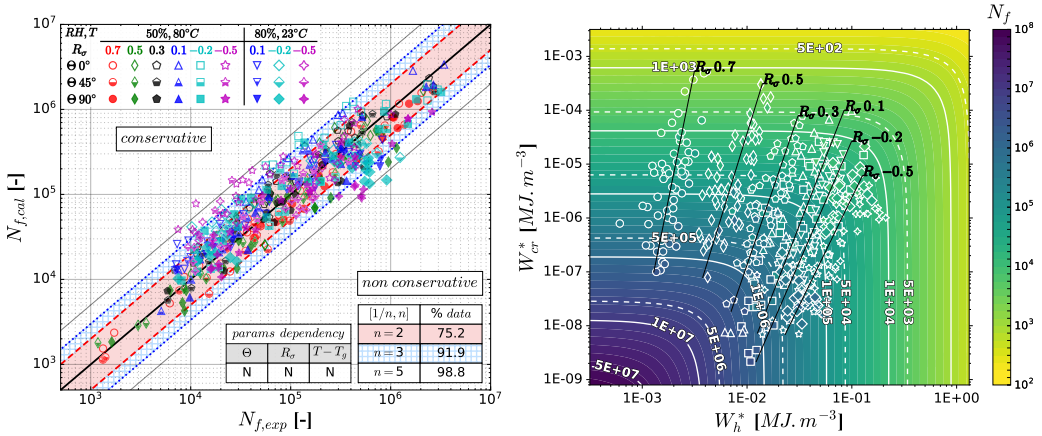

(a) (b)

Figure 21: Performance of the proposed criterion based on the creep and hysteresis energies: (a) comparison between the predicted fatigue life and the experimental one, (b) shape of the fatigue lifetime isolines.

Variant 2. The second criterion is based on the creep energy density and on the cyclic energy density. The advantage of this criterion is that the calculation of cyclic energy density requires simpler mechanical models than hysteresis energy density. The same form is kept:

$$\frac{1}{N_f} = \left(\frac{W_{cr}^\star}{A_2}\right)^{b_2} + \left(\frac{W_c^\star}{C_2}\right)^{d_2} \tag{22}$$

Fig. 22a shows that this criterion provides the best results, with 97% of data within a scatter band of a factor 3. It also exhibits fully consistent results in terms of fatigue life isolines (see Fig. 22b).

5. Criteria performance and discussion

5.1. Comparison of the criteria

A large number of criteria was investigated in this study and this section is dedicated to discuss their performances. To ease the comparison, only the percentage of data within the scatter bands of factor 3 are kept and plotted simultaneously in Fig. 23. Considering first a global identification, *i.e.* a single set of parameters is used to fit the whole database. Fig. 23a

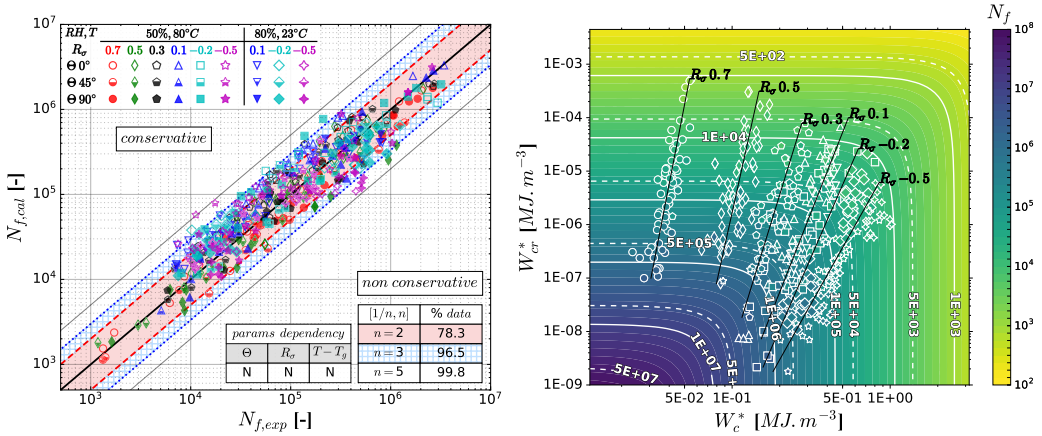

(a) (b)

Figure 22: Performance of the proposed criterion based on the creep and cyclic energies: (a) comparison between the predicted fatigue life and the experimental one, (b) shape of the fatigue iso-lifetime.

clearly shows that criteria based on a single variable are not able to take into account, with a single set of parameters, the effects of load ratio, orientation and environment. The modified Gerber criterion and the criteria based on the cyclic strain rate differ from the rest of this kind of criteria. In the case of the Gerber model, a multi-identification is used, which biases the results. Considering the criteria based on the cyclic mean strain rate, their good behavior is only apparent as they are not able to capture the load ratio effect for negative load ratios.

A possible way to enhance these criteria is to adjust their parameters depending on some variables (mainly the load ratio). Fig. 23b sums up what can be done with these criteria. The dependency of the parameters to the variables is indicated in brackets. With more numerous parameters, the predictions are of course improved and single variable cyclic strain rate and creep energy criteria could reach the performance of mixed criteria.

The mixed criteria present a significant improvement over the single variable criteria, with a single set of parameters for each criterion. Recent criteria from Raphael *et al.* [23] provide a very good description of the full database but the evaluations of the fatigue life isolines have to be considered carefully as detailed in Section 4.2.1. The two IDAFIP criteria presented in this article lead to a very good description of the full database. Variant 2 (Section

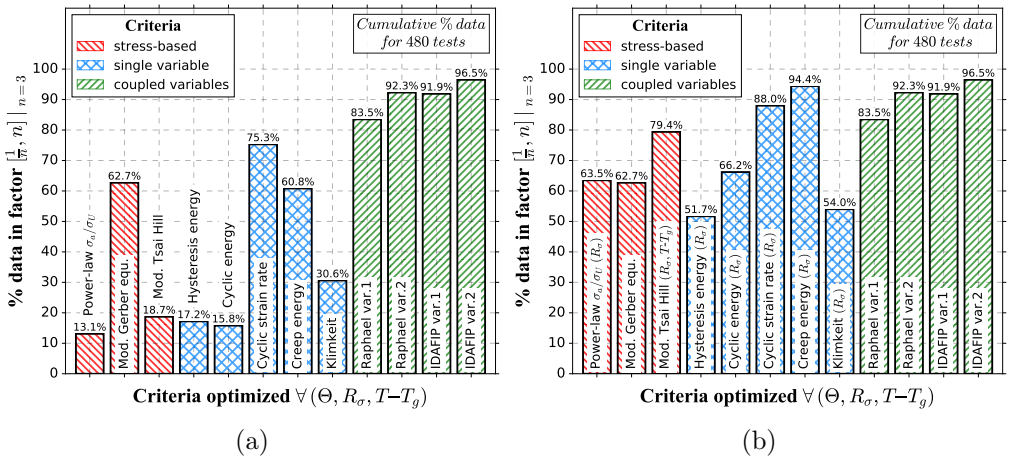

(a) (b)

Figure 23: Percentage of fatigue life predicted by the criteria within a scatter band with a factor 3 by using (a) constant parameters (*i.e.* without additional dependency to Θ, R_σ and $T - T_g$) and (b) parameters depending on some variable(s) (additional dependency indicated in parentheses).

4.2.2) requires a less complex constitutive model, as a simple linear elastic approach with a capability to capture the cyclic ratcheting is enough, whereas a complex model able to capture the cyclic response is needed for variant 1.

5.2. Minimal experimental database

From an industrial point of view, the generation of such an extensive experimental database cannot be systematically performed for every material. The question of the minimum experimental database needed to identify the parameters is therefore of high interest. In this section, the variant 2 of the IDAFIP criterion will be used to investigate the optimal downsizing of the identification database for various combinations of different load ratios and orientations. The percentage of data within the scatter bands of factor 3 is evaluated for each configuration.

Fig. 24 compares the accuracy of the predictions obtained for several combinations of two load ratios. The intuition would lead to consider at least one positive and one negative load ratio. The results actually show that this condition is relevant but is not mandatory, as long as a good balance between the evolutions of the cyclic and creep energies is provided by the selected load ratios. This is especially illustrated by the good results obtained for the load ratios $\{-0.5, -0.2\}$ (Figs. 22b and 24).

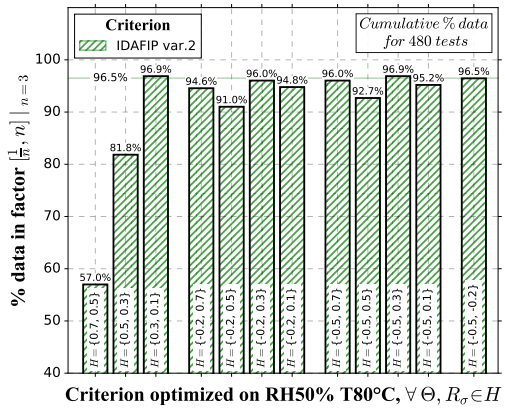

Figure 24: Percentage of fatigue life (all data included) predicted within a scatter band with a factor 3 by variant 2 of the IDAFIP criterion identified over a reduced database including three orientations and only one atmospheric condition (RH50% T80°C) and two load ratios (put into braces) (the horizontal line at 96.5% corresponds to the prediction obtained when parameters identification is based on all the database).

Fig. 25 investigates the accuracy of the predictions obtained when a limited amount of orientations is considered. The best combination of load ratios selected from the previous study are considered, *i.e.* $\{0.1, 0.3\}$, $\{-0.2, 0.3\}$, $\{-0.5, 0.3\}$ and $\{-0.5, -0.2\}$. Performing an identification for only one sample orientation reduces sensibly the accuracy of the predictions. Performing the identification on two orientations $\{0°, 90°\}$ or $\{45°, 90°\}$ leads to almost the same accuracy than an identification performed over the three orientations (*i.e.* including the results on 0°, 45° and 90° samples).

6. Conclusions

In this paper, an extended fatigue database (480 tension-compression tests) obtained on Polyamide 66 reinforced with 50% of glass fibers (PA66 GF50) is presented. The fatigue results are obtained for a wide range of load ratios (from -0.5 to 0.7), three orientations (0°, 45° and 90°) and two environmental conditions (RH50%, T80°C and RH80% T23°C). Beyond sharing these experimental results, another objective of this paper was to compare the ability of numerous fatigue criteria to provide a robust description of the fatigue database, possibly with a unified set of parameters. Additionally to existing criteria, this paper also defined two original models, based on the combination of the creep energy density and of an evaluation of the cyclic

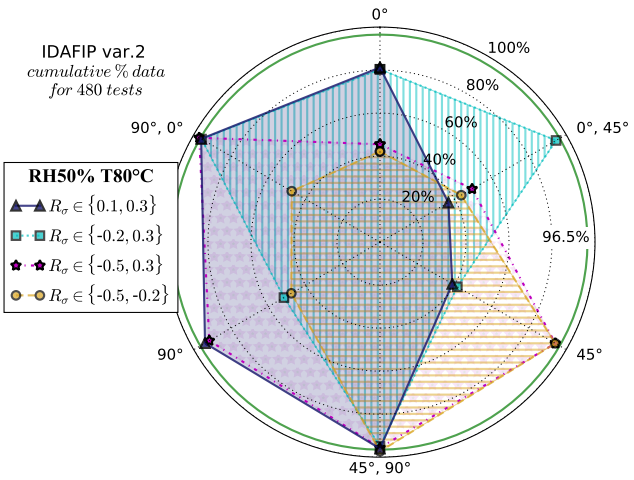

Figure 25: Percentage of fatigue life (all data included) predicted within a scatter band with a factor 3 by variant 2 of the IDAFIP criterion identified over a reduced database including only one atmospheric condition (RH50% T80°C) and one, two or three orientations, for several sets of two load ratios (the green line at 96.5% corresponds to the prediction obtained when parameters identification is based on all the database).

(elastic or anelastic) energy. Most of classic criteria were not able to describe accurately the whole database. In the discussion section, the performances obtained for a single set of parameters and for different sets of parameters (*i.e.* the highest criterion's performance) are presented. The main observations are the following:

- Criteria based on stress components manage to unify rather well the orientations and environments effects as soon as they are formulated with a ratio to the ultimate stress at break. Nevertheless, they clearly fail to unify the influence of load ratio with a single set of parameters. When leaving some freedom on the dependency on load ratios, results improve but stay below 80% of data points unified within a scatter with a ratio of 3.

- Models based on ratcheting effect (cyclic creep increment or creep energy density) can give indeed very good results (almost 90% of unification for a scatter within a factor by 3 for creep energy density) but fail systematically to unify the tests performed for negative load ratios.

- Criteria based on the cyclic loop energy densities (elastic or anelastic),

can give good results but fail to describe high positive load ratios, exhibiting a significant ratcheting and inducing an earlier failure.

- Criteria mixing ratcheting and cyclic features are clearly the best ones to provide a very good description of the full database for a unified set of parameters. Within this family, two variants of a criterion published very recently [23] that combines cyclic strain rate and hysteresis energy density were first considered. Both variants are giving good results (over 80% of the database unified within a scatter of a factor by 3). However a plot in the space of (cyclic strain rate; hysteresis energy density) exhibited that the shapes of the iso-lifetime curves are either too sharp (variant based on the minimum of the two components) or leading to unphysical evolutions for more negative load ratios (variant with nonlinear coefficient).

- Two original criteria called IDAFIP were defined in this paper. The first variant is combining the creep energy density (defined as the product of the mean stress multiplied by the stabilized cyclic strain rate) to the hysteresis energy density. The second one is combining the same creep energy density to the cyclic energy density (defined as half the product of strain amplitudes times the stress amplitude). Both variants lead to a very good unification of the database for only 4 parameters (over 90% of the database is unified within a scatter of a ratio of 3). The variant using the creep energy density and the cyclic energy density gives the best results and is moreover very interesting from a design point of view because it requires less complex models to predict the cyclic energy density rather than the anelastic one.

This study allowed identifying the set of parameters for the fatigue criteria over a very wide database. The generation of such an experimental database clearly requires huge efforts on samples generation, conditioning, tests duration and data treatment. Taking advantage of this extended database, an interesting question is dealing with downsizing the database needed for the relevant identification of the criterion parameters. A last section therefore investigates the minimum experimental database (various orientations, load ratios, orientations) needed for the parameters identification, to describe accurately the full database. The investigations were achieved with the IDAFIP criterion based on creep energy density and cyclic energy density. The conclusions are the following:

- In this range of temperature $[T_g + 30°\text{C}; T_g + 45°\text{C}]$, it seems that one of the atmospheric condition is enough to get a good evaluation of the parameters for the other one.
- Performing an identification for only one sample orientation reduces substantially the accuracy of the predictions. Performing the identification on two orientations $\{0°, 90°\}$ or $\{45°, 90°\}$ leads to almost the same accuracy as an identification performed over the three orientations (*i.e.* including the results on 0°, 45° and 90° samples).
- As illustrated previously, the most difficult parameter to identify is the influence of the load ratio. The results obtained showed that an identification performed on only two load ratios can give very good results (comparable to the identification on the full set of load ratios), provided that the two load ratios lead to reasonable combined variations of creep and cyclic energies. Very good results were therefore obtained for combinations of one positive and one negative load ratio, which was somehow expected, but also for the couple of load ratios $\{-0.5, -0.2\}$ because they provide a good balance of the variations of creep and cyclic energies for the range of fatigue lifetime investigated.

Perspectives to this work are numerous. The first ones would be to investigate the extension of these conclusions to other materials (filled or unfilled polymers) or to other environments (closer or below T_g). Then, this study only considered uniaxial loading, which is of course a limited field for structures design. It will therefore be necessary to extend the IDAFIP criterion to multiaxial cases. If cyclic energy density should not be too much of an issue as illustrated by some studies [21], the computation of the creep energy density will require careful considerations on the norms used to evaluate both stress and cyclic strain rate components. The last perspective would be to use the criterion identified to design a structure (complex sample or industrial parts) and to check how well the approach applies in the case of complex microstructure and loading.

Acknowledgements

This work was performed in the framework of the IDAFIP project. It has received the financial support from the French National Association for Technical Research. The authors are grateful to Vibracoustic and Solvay Performance Polyamides for their support throughout.

References

[1] Y. Marco, V. Le Saux, L. Jégou, A. Launay, L. Serrano, I. Raoult, S. Calloch, Dissipation analysis in SFRP structural samples: Thermomechanical analysis and comparison to numerical simulations, International Journal of Fatigue 67 (2014) 142–150.

[2] V. Zobel, M. Stommel, G. Scheuermann, Feature-based tensor field visualization for fiber reinforced polymers, in: 2015 IEEE Scientific Visualization Conference (SciVis), 2015, pp. 49–56.

[3] A. Bernasconi, F. Cosmi, E. Zappa, Combined effect of notches and fibre orientation on fatigue behaviour of short fibre reinforced polyamide, Strain 46 (5) (2010) 435–445.

[4] Y. Zhou, P. K. Mallick, Fatigue performance of an injection-molded short e-glass fiber-reinforced polyamide 6,6. I. effects of orientation, holes, and weld line, Polymer Composites 27 (2) (2006) 230–237.

[5] L. Serrano, Y. Marco, V. Le Saux, G. Robert, P. Charrier, Fast prediction of the fatigue behavior of short-fiber-reinforced thermoplastics based on heat build-up measurements: application to heterogeneous cases, Continuum Mechanics and Thermodynamics 29 (5) (2017) 1113–1133.

[6] A. Launay, Y. Marco, M. H. Maitournam, I. Raoult, Influence of temperature and relative humidity on the cyclic behaviour of a short glass fibre reinforced polyamide, Mechanics of Materials 56 (2013) 1–10.

[7] G. Meneghetti, M. Ricotta, G. Lucchetta, S. Carmignato, An hysteresis energy-based synthesis of fully reversed axial fatigue behaviour of different polypropylene composites, Composites Part B: Engineering 65 (2014) 17–25.

[8] S. Mortazavian, A. Fatemi, Fatigue behavior and modeling of short fiber reinforced polymer composites: A literature review, International Journal of Fatigue 70 (2015) 297–321.

[9] A. K. Shojaei, A. R. Wedgewood, An anisotropic cyclic plasticity, creep and fatigue predictive tool for unfilled polymers, Mechanics of Materials 106 (2017) 20–34.

[10] A. Bernasconi, P. Davoli, A. Basile, A. Filippi, Effect of fibre orientation on the fatigue behaviour of a short glass fibre reinforced polyamide-6, International Journal of Fatigue 29 (2) (2007) 199–208.

[11] M. D. Monte, E. Moosbrugger, M. Quaresimin, Influence of temperature and thickness on the off-axis behaviour of short glass fibre reinforced polyamide 6.6 – cyclic loading, Composites Part A: Applied Science and Manufacturing 41 (10) (2010) 1368–1379.

[12] S. Barbouchi, V. Bellenger, A. Tcharkhtchi, P. Castaing, T. Jollivet, Effect of water on the fatigue behaviour of a pa66/glass fibers composite material, Journal of Materials Science 42 (6) (2007) 2181–2188.

[13] N. Jia, V. A. Kagan, Effects of time and temperature on the tension-tension fatigue behavior of short fiber reinforced polyamides, Polymer Composites 19 (4) (1998) 408–414.

[14] A. Zago, G. S. Springer, Constant amplitude fatigue of short glass and carbon fiber reinforced thermoplastics, Journal of Reinforced Plastics and Composites 20 (7) (2001) 564–595.

[15] A. Bernasconi, R. M. Kulin, Effect of frequency upon fatigue strength of a short glass fiber reinforced polyamide 6: A superposition method based on cyclic creep parameters, Polymer Composites 30 (2) (2009) 154–161.

[16] M. Eftekhari, A. Fatemi, On the strengthening effect of increasing cycling frequency on fatigue behavior of some polymers and their composites: Experiments and modeling, International Journal of Fatigue 87 (2016) 153–166.

[17] J. A. Sauer, A. D. McMaster, D. R. Morrow, Fatigue behavior of polystyrene and effect of mean stress, Journal of Macromolecular Science, Part B 12 (4) (1976) 535–562.

[18] P. Mallick, Y. Zhou, Effect of mean stress on the stress-controlled fatigue of a short e-glass fiber reinforced polyamide-6,6, International Journal of Fatigue 26 (9) (2004) 941–946.

[19] C. Sonsino, E. Moosbrugger, Fatigue design of highly loaded short-glass-fibre reinforced polyamide parts in engine compartments, International Journal of Fatigue 30 (7) (2008) 1279–1288.

[20] A. Launay, M. Maitournam, Y. Marco, I. Raoult, Multiaxial fatigue models for short glass fiber reinforced polyamide – part I: Nonlinear anisotropic constitutive behavior for cyclic response, International Journal of Fatigue 47 (2013) 382–389.

[21] A. Launay, M. Maitournam, Y. Marco, I. Raoult, Multiaxial fatigue models for short glass fibre reinforced polyamide. part II: Fatigue life estimation, International Journal of Fatigue 47 (2013) 390–406.

[22] S. Mortazavian, A. Fatemi, Fatigue behavior and modeling of short fiber reinforced polymer composites including anisotropy and temperature effects, International Journal of Fatigue 77 (2015) 12–27.

[23] I. Raphael, N. Saintier, H. Rolland, G. Robert, L. Laiarinandrasana, A mixed strain rate and energy based fatigue criterion for short fiber reinforced thermoplastics, International Journal of Fatigue 127 (2019) 131–143.

[24] J. Bowman, M. B. Barker, A methodology for describing creep-fatigue interactions in thermoplastic components, Polymer Engineering & Science 26 (22) (1986) 1582–1590.

[25] H. Oka, R. Narita, Y. Akiniwa, K. Tanaka, Effect of mean stress on fatigue strength of short glass fiber reinforced polybuthyleneterephthalate, Key Engineering Materials 340 (2007) 537–542.

[26] M. Eftekhari, A. Fatemi, Creep-fatigue interaction and thermo-mechanical fatigue behaviors of thermoplastics and their composites, International Journal of Fatigue 91 (2016) 136–148.

[27] A. Constantinescu, K. Dang Van, M. H. Maitournam, A unified approach for high and low cycle fatigue based on shakedown concepts, Fatigue & Fracture of Engineering Materials & Structures 26 (6) (2003) 561–568.

[28] A. Benoit, M. Maitournam, L. Rémy, F. Oger, Cyclic behaviour of structures under thermomechanical loadings: Application to exhaust manifolds, International Journal of Fatigue 38 (2012) 65–74.

[29] J. J. Horst, Influence of fibre orientation on fatigue of short glass fibre reinforced polyamide, Ph.D. thesis, Delft University of Technology, Nederland (1997).

[30] E. Seignobos, Compréhension des mécanismes physiques de fatigue dans le polyamide vierge et renforcé de fibres de verre, Ph.D. thesis, INSA Lyon, France (2009).

[31] D. Kujawski, F. Ellyin, A unified approach to mean stress effect on fatigue threshold conditions, International Journal of Fatigue 17 (2) (1995) 101–106.

[32] B. Klimkeit, Y. Nadot, S. Castagnet, C. Nadot-Martin, C. Dumas, S. Bergamo, C. Sonsino, A. Büter, Multiaxial fatigue life assessment for reinforced polymers, International Journal of Fatigue 33 (6) (2011) 766–780.

[33] S. Amiable, S. Chapuliot, A. Constantinescu, A. Fissolo, A comparison of lifetime prediction methods for a thermal fatigue experiment, International Journal of Fatigue 28 (7) (2006) 692–706.

[34] L. Jegou, Y. Marco, V. Le Saux, S. Calloch, Fast prediction of the wöhler curve from heat build-up measurements on short fiber reinforced plastic, International Journal of Fatigue 47 (2013) 259–267.

[35] G. Meneghetti, M. Quaresimin, Fatigue strength assessment of a short fiber composite based on the specific heat dissipation, Composites Part B: Engineering 42 (2) (2011) 217–225.

[36] C. Guevenoux, Critère de fatigue des thermoplastiques renforcés en fibres de verres courtes, Master's thesis, Ecole Polytechnique, France (2016).

[37] L. Leveuf, L. Navrátil, V. Le Saux, Y. Marco, J. Olhagaray, S. Leclercq, Constitutive equations for the cyclic behaviour of short carbon fibre-reinforced thermoplastics and identification on a uniaxial database, Continuum Mechanics and Thermodynamics.

[38] N. Billon, L. Silva, A. Andriyana, Mechanical response of a short fiber-reinforced thermoplastic: Experimental investigation and continuum mechanical modeling, European Journal of Mechanics-A/Solids 29 (6) (2010) 1065–1077.

[39] A. Krairi, I. Doghri, A thermodynamically-based constitutive model for thermoplastic polymers coupling viscoelasticity, viscoplasticity and ductile damage, International Journal of Plasticity 60 (2014) 163–181.

[40] A. Krairi, I. Doghri, G. Robert, Multiscale high cycle fatigue models for neat and short fiber reinforced thermoplastic polymers, International Journal of Fatigue 92 (2016) 179–192.

[41] F. Meraghni, H. Nouri, N. Bourgeois, C. Czarnota, P. Lory, Parameters identification of fatigue damage model for short glass fiber reinforced polyamide (PA6-GF30) using digital image correlation, Procedia Engineering 10 (2011) 2110–2116.

[42] A. Krairi, I. Doghri, Multi-scale damage model for mechanical high cycle fatigue (HCF) of short glass fibre reinforced thermoplastics (SGFRTP), Procedia Engineering 66 (2013) 759–765.

[43] M. Arif, N. Saintier, F. Meraghni, J. Fitoussi, Y. Chemisky, G. Robert, Multiscale fatigue damage characterization in short glass fiber reinforced polyamide-66, Composites Part B: Engineering 61 (2014) 55–65.

[44] H. Rolland, N. Saintier, I. Raphael, N. Lenoir, A. King, G. Robert, Fatigue damage mechanisms of short fiber reinforced PA66 as observed by in-situ synchrotron x-ray microtomography, Composites Part B: Engineering 143 (2018) 217–229.

[45] I. Raphael, N. Saintier, G. Robert, J. Béga, L. Laiarinandrasana, On the role of the spherulitic microstructure in fatigue damage of pure polymer and glass-fiber reinforced semi-crystalline polyamide 6.6, International Journal of Fatigue 126 (2019) 44–54.

[46] L. Serrano, Thermomechanical characterization of the fatigue behaviour of short fibers reinforced thermoplastic, Ph.D. thesis, Université de Bretagne occidentale, France (2015).

[47] M. Broudin, P. L. Gac, V. Le Saux, C. Champy, G. Robert, P. Charrier, Y. Marco, Water diffusivity in PA66: Experimental characterization and modeling based on free volume theory, European Polymer Journal 67 (2015) 326–334.

[48] Y. L. Chenadec, I. Raoult, C. Stolz, T. M.-L. Nguyen-Tajan, Cyclic approximation of the heat equation in finite strains for the heat build-up problem of rubber, Journal of Mechanics of Materials and Structures 4 (2009) 309–318.

[49] F. Ellyin, Fatigue Damage, Crack Growth and Life Prediction, Springer Netherlands, Dordrecht, 1997.